Helmholtz-Zentrum Dresden-Rossendorf (HZDR)

MoS$_2$ quantum dots as an efficient catalyst material for oxygen evolution reaction

MoS$_2$ Quantum Dots as an Efficient Catalyst Material for Oxygen Evolution Reaction

Bishnupad Mohanty,[1,9] Mahdi Ghorbani-Asl,[3*] Silvan Kretschmer,[3] Arnab Ghosh,[5,7] Puspendu Guha,[5,6] Subhendu K. Panda,[8] Bijayalaxmi Jena,[9] Arkady V. Krasheninnikov,[3,4,10*] Bikash Kumar Jena[1,2*]

[1]CSIR-Institute of Minerals and Materials Technology, Bhubaneswar-751013, India.

[2]Academy of Scientific & Innovative Research, New Delhi-110001, India.

[3]Helmholtz-Zentrum Dresden-Rossendorf, Institute of Ion Beam Physics and Materials Research, 01328 Dresden, Germany

[4] Department of Applied Physics, Aalto University School of Science, PO Box 11100, 00076 Aalto, Finland

[5]Institute of Physics, Bhubaneswar-751005, India.

[6] Homi Bhabha National Institute, Training School Complex, Anushakti Nagar, Mumbai 400085, India

[7]Department of Physics, Indian Institute of Technology Kharagpur, Kharagpur 721302, India

[8]CSIR-Central Electrochemical Research Institute, Karaikudi – 630003, India

[9]Department of Chemistry, Utkal University, Bhubaneswar-751004, Odisha, India.

[10]National University of Science and Technology MISiS, 119049 Moscow, Russia.

ABSTRACT: The development of an active, earth-abundant and inexpensive catalyst for oxygen evolution reaction (OER) is highly desirable, but remains a great challenge. Here, by combining experiments and first-principles calculations, we demonstrate that MoS$_2$ quantum dots (MSQDs) are an efficient material for OER. We use a simple route for the synthesis of MSQDs from a single precursor in aqueous medium avoiding the formation of unwanted carbon quantum dots (CQDs). The as-synthesized MSQDs exhibit higher OER activity with the lower Tafel slope as compared to that for the state-of-the-art catalyst IrO$_2$/C. The potential cycling of the MSQDs activates the surface and improves the OER catalytic properties. The density functional theory calculations reveal that MSQD vertices are reactive and the vacancies at the edges also promote the reaction, which indicates that the small flakes with defects at the edges are efficient for OER. The presence of CQDs affects the adsorption of reaction intermediates and dramatically suppresses the OER performance of the MSQDs. Our theoretical and experimental findings provide important insights into the synthesis process of MSQDs and their catalytic properties and suggest promising routes to tailoring the performance of the catalysts for OER applications.

The concerns over the hasty depletion of fossil fuels, the cumulative increase in the energy consumption, and the associated ecological issues have compelled the society to explore new energy resources, especially for automotive industries. Combined with the energy harvested from the sun and wind, water is the best renewable resource to produce fuel and minimize the effects of fossil fuels on the environment.[1-3] No surprise that the process of water splitting to hydrogen (H$_2$) and oxygen (O$_2$) has attracted substantial attention as a clean and eco-friendly energy source. The hydrogen evolution reaction (HER) is important for the generation of the cleanest fuels, while the oxygen evolution reaction (OER) is equally important for fuel cells and metal-air batteries.[4,5] Compared to the HER, OER involves a multistep (proton coupled with 4 electrons) oxidation process and gives sluggish electrode kinetics.[6] The state-of-the-art Ir and Ru-based catalysts give the higher rate for the OER process, but scarcity and the high cost of these materials limit their practical applications.[7,8] Therefore, the search for new and efficient catalysts to accelerate this inherently sluggish kinetics by decreasing the overpotential and increasing the rate of conversion is of great importance, and lots of effort has recently been focused on transition metal-based electrocatalysts, like metal oxides,[9,10] phosphides,[11-14] sulphides,[15-17] and selenides[18-20] for HER and OER due to their high catalytic stability and abundance.

At the same time, two-dimensional (2D) transition metal dichalcogenides (TMDs) such as MoS$_2$, WS$_2$, MoSe$_2$ have recently received an enormous amount of attention[21-24] in the context of catalysis due to their very morphology and reduced dimensionality, as well as chemical properties. Specifically, MoS$_2$ has been extensively studied as a unique electrocatalyst for HER.[25,26] The activity of MoS$_2$ and other TMDs towards OER has also been investigated[27,28]. It has been demonstrated that sulfur-terminated edges of MoS$_2$ flakes are catalytically very active.[29] Therefore, nanostructures like quantum dots (QDs) of MoS$_2$ must be favored as the efficient materials over their bulk counterparts. The electrochemical HER on MoS$_2$ QDs (MSQDs) has been thoroughly studied,[30,31] but the performance of the MSQDs towards OER has not yet been explored. Moreover, the synthesis of MSQDs is normally done in the presence of carbon (organic) solvents.[32] This leads to the formation of unavoidable carbon QDs (CQDs) and ultimately may interfere with the properties and performance of MSQDs.

In this report, a single-step hydrothermal synthesis technique has been developed using a single precursor

$((NH_4)_2MoS_4)$ avoiding the carbon source (organic) solvents, as schematically shown in Figure 1. The resultant MSQDs exhibits excellent electrocatalytic activity towards OER due to reactive sites, including vertices and defects at MS₂ edges, as confirmed by our first-principles calculations. The surface of MSQDs was activated by potential cycling to explore the performance. For comparison, the MSQDs have also been synthesized in the presence of an organic solvent (DMF) to produce the mixture of MoS_2 and carbon QDs (MSQDs@CQDs) under similar synthesis condition. The electrocatalytic activity has been analyzed to reveal the influence of the unavoidable CQDs on the OER performance of sole MSQDs.
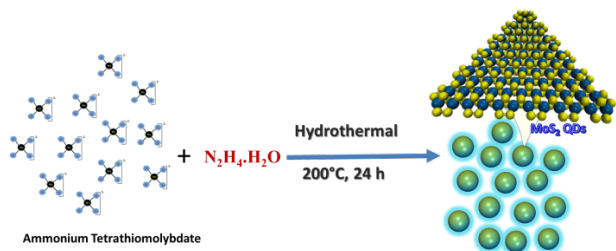

Figure 1. Schematic representation of the MSQDs synthesis. Ammonium tetrathiomolybdate was used as a single precursor for MoS_2 growth.

A single precursor, ammonium tetrathiomolybdate, was used as the source for both Mo and S. The hydrazine was utilized as the reducing agent for the formation of MoS_2. The possible reaction in the formation of MoS_2 from $(NH_4)_2MoS_4$ in the presence of hydrazine is presented in equation 1.[33]

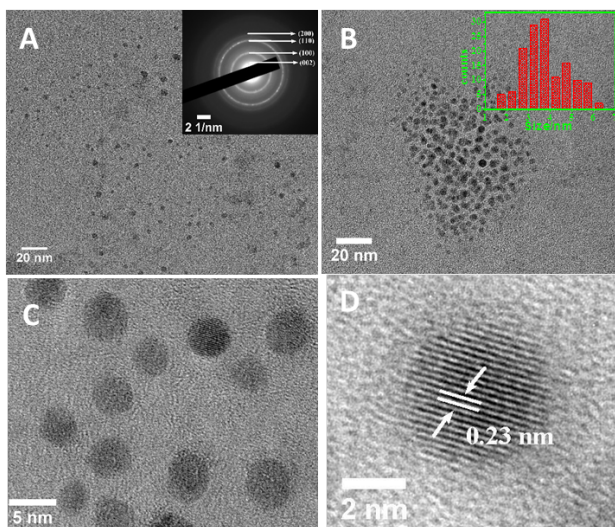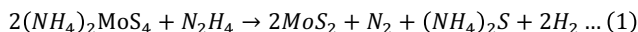$$2(NH_4)_2MoS_4 + N_2H_4 \rightarrow 2MoS_2 + N_2 + (NH_4)_2S + 2H_2 \dots (1)$$

Figure 2. (A, B) TEM, (C, D) HRTEM images of MSQDs. The inset in panel (A) is the selected area electron diffraction patterns of MSQDs. The inset in panel (B) shows the statistical analysis of size distribution of the as-synthesized MSQDs.

The details of the synthesis process are given in the supporting information. After formation of MSQDs, the high-resolution TEM (HRTEM) was used to characterize their sizes and morphology (Figure 2). As evident from Fig. 2B, the as-synthesized MSQDs are rather narrow in size distribution. Most of the particles have sizes less than 5 nm with very low aggregation. The HRTEM image shows the lattice spacing of

2.3Å which is assigned to (110) plane of a hexagonal pattern of MoS_2.[34] The selected area electron diffraction pattern indicates that the MSQDs are crystalline in nature.[35] The atomic valence state and chemical composition measurement were carried out by X-ray photoelectron spectroscopy (XPS) (Figure S1). The high-resolution XPS of Mo 3d region in MSQDs was de-convoluted into two main intense peaks at 232 eV and 235 eV that correspond to the Mo $3d_{5/2}$ and Mo $3d_{3/2}$ signatures thus revealing the presence of mixed valences of +4 and +5 states of Mo. A similar observation has been documented by the Shaijumon's group.[30] This indicates that the edges of the MSQDs are slightly oxidized being usually in contact with water and atmosphere. The above conclusion has been con-
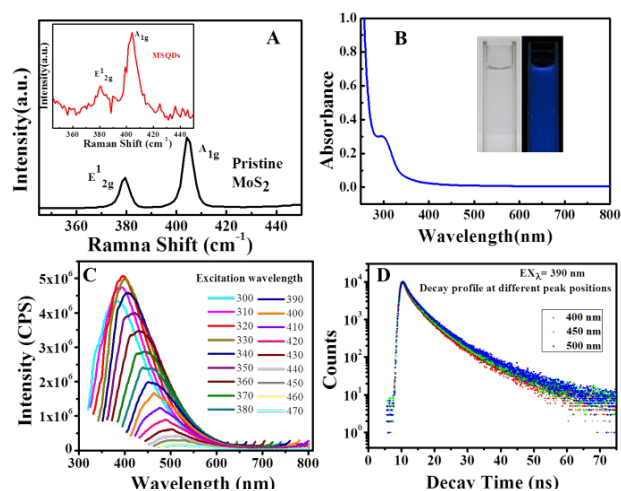

Figure 3. (A) Raman spectra of pristine MoS_2 (inset shows the Raman spectra of MSQDs), (B) UV-visible spectra of MSQDs (inset shows the images before and after irradiation of UV light of 365 nm lamp), (C) shows the PL spectrum of MSQDs excited at different wavelengths and (D) represents the fluorescence lifetime spectrum at different emission wavelengths.

firmed by the findings of the peak at 168 eV, which points to the presence of S-O bonds.[36] The Raman spectroscopy experiments were carried out to compare the spectra of the as-synthesized MSQDs with those of the pristine MoS_2 (Figure 3A). The pristine MoS_2 shows two strong characteristic peaks at around 379.3 cm⁻¹ and 404.5 cm⁻¹ associated with the in-plane E^1_{2g} and out-of-plane A_{1g} vibrational mode of Mo-S bond, respectively.[37] Frequency, intensity, and width of the peak observed for E^1_{2g} and A_{1g} vibrational modes reflects the layer thickness of the MoS_2.[38] The as-synthesized MSQDs shows E^1_{2g} and A_{1g} vibrational modes at around 380 and 403.3 cm⁻¹ respectively. Interestingly, it has been observed that the MSQDs exhibit a redshift of E^1_{2g} and blue shift of A_{1g} vibrational modes, as compared to the pristine MoS_2. This confirms that the as-synthesized MSQDs consists of a few layers of MoS_2. This is in agreement with the similar observations reported by Lee et al.[39] The intensity ratio of the A_{1g} and E^1_{2g} modes was derived to deduce the texture information of the as-synthesized MSQDs. The A_{1g}/ E^1_{2g} ratio of MSQDs possess a higher value of 3.32 as compared to the pristine MoS_2 (2.36) that evidently reflects the higher edge-terminated structure.[40]

The UV-visible spectrum of the as-prepared MSQDs gives a single peak near UV-region at 300 nm (Figure 3B). MSQD solution displays blue fluorescence on irradiation with a 365 nm UV lamp (Inset of Figure 3B). This absorption peak at 300 nm was assigned as the signature of the excitonic features of MSQDs.[41] The small size MSQDs cause the quantum confinement effect, which leads to an increase in the band gap. The gap was estimated to be around 3.73 eV, which is much higher than that of bulk MoS_2 (1.2 eV) and monolayer MoS_2 (1.9) eV.[42] The high uniformity of size and thickness of MSQDs would produce an inherent photoluminescence (PL) spectrum. Therefore, the PL spectra of MSQDs dispersions were recorded at different wavelengths (Figure 3C). The increase in excitation wavelength led to the red shift in the luminescence emission spectra, and it was observed over the wavelengths ranging from nearly 350 nm to 550 nm. The obtained broad peak may be attributed to the direct band-edge recombination. The excitation-dependent luminescence indicates polydispersity in the lateral dimension of the MSQDs dispersions.[43] The red-shift in the emission is likely due to the formation of deeper trap states for the uncompensated sulfide ions and metal ions on the surface of the QDs. The excitation at 320 nm shows the maximum peak intensity at 400 nm, and that the peak intensity was observed to decrease with increasing the excitation wavelength. This gives the particle size distribution which agrees well with the TEM observations.[44] To understand the nature of the recombination processes of the MSQDs, the fluorescence lifetime spectra were taken at different emission wavelengths. All are fitted well to a 3rd-order exponential decay profile with the average reduced weighted chi-squared residual (χ^2) value of <1.2. The calculated values are given in Table S1. Interestingly, not much change in the emission decay lifetimes was observed for the QDs indicating that the nature of electronic relaxation is the same for various sizes of QDs present in the as-synthesized sample. The average excitation lifetime for the MSQDs was found in the range of 10 nanoseconds. Since the edge emission of recombining electron/hole pairs for MoS_2 has a characteristic time of several picoseconds or less, it is reasonable to assign the observed long-lived emission of MSQDs to charge recombination through defect states that exist mostly on the edges of the QDs.[45]

Having characterized the synthesized MSQDs, we proceed to the study of their OER properties. The catalyst was modified over the glassy carbon (GC) working electrode. The OER polarization curves were recorded by linear sweep voltammetry (LSV) at a scan rate of 5 mV/s in 1 M KOH. The control experiment on GC was also performed for verification. The benchmark experiments on catalyst IrO_2/C and pristine MoS_2 were carried out for comparison. All the polarization curves were iR corrected, and the LSV plots are shown in Figure 4A. The IrO_2/C catalyst exhibited higher OER activity with lower overpotential.[46] The bare GC electrode and the pristine MoS_2 shows poor catalytic activity, while MSQDs demonstrated enhanced OER activity with lower overpotential and higher current density. Further, the hydrothermal condition was optimized by checking the OER performance of as-synthesized MSQDs obtained with varying the reaction temperature and duration of reaction (Figure S2). Then, the activation of the QDs has been carried out by potential cycling the modified electrode in the electrolyte conditions. The optimization of the activation process was checked from the OER polarization LSV response (Figure S3). It has been observed that the catalytic current density increases with the number of potential cycles. However, no further enhancement of the current density was observed beyond 50 potential cycles. The activation cycling probably increases the number of active sites of the MSQDs and makes them catalytically more active. The as-synthesized materials after cycling (MSQDs-AC) gives higher activity, as compared to that before cycling (MSQDs) with a lower onset overpotential of 280 mV. The interesting enhancement of the OER activity after cycling was further accessed by the impedance measurement (Figure 4C). The MSQDs-AC shows a lower value of charge transfer resistance in the Nyquist plot as compared to MSQDs. The better charge transfer resistance and higher metallic character in MSQDs-AC reflect the better performance in OER activity. The detailed mechanism of activation is not fully understood at this point and needs further study. The MSQDs-AC achieved a current density of 10 mA/cm^2 and 100 mA/cm^2 at the overpotential of 370 mV and 570 mV, respectively. This overpotential value is much smaller as compared to the pristine MoS_2. This suggests that the MSQDs are highly active for OER.
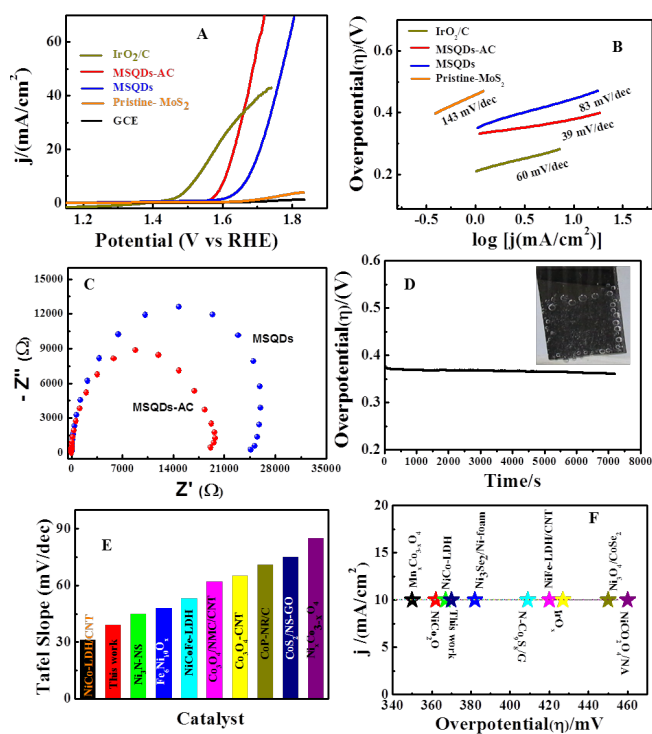

Figure 4. (A) LSV polarization plot towards OER for different electrocatalysts on glassy carbon electrode in 1 M KOH at a scan rate of 5 mV/s. (B) Corresponding Tafel plots. (C) Nyquist plot of MSQDs before and after activation through potential cycling (D) Chronopotemetric measurement for MSQDs-AC modified electrode at a constant current density of 10 mA/cm^2 (Inset image shows the evolution of oxygen bubbles on the surface of the catalysts). (E) The comparison of onset overpotential towards OER with other reported catalysts and (F) Comparison of overpotential to generate 10 mA/cm^2 on different catalysts towards OER.

It is worth to compare the onset overpotential and the overpotential required to generate the benchmark current density (10 mA/cm^2) for present MSQDs with various other catalysts (Figure 4E &D). Nevertheless, the as-synthesized MSQDs shows lower activity as compared to the state-of-art catalyst

IrO$_2$/C. However, taking into account the cost and scarcity of Ir, it can be compensated by the lower cost, higher abundance and easy production of MSQDs-based catalysts. The kinetics of the as-synthesized materials towards the OER was investigated by measuring Tafel polarization plot, i.e. the plot of "overpotential (η) vs log j". Figure 4B represents the Tafel plot for pristine MoS$_2$, MSQDs after and before cycling (MSQDs-AC and MSQDs) and IrO$_2$/C. The Tafel slope of MSQDs-AC was estimated to be 39 mV/dec, which is much lower than for the pristine MoS$_2$ (143 mV/dec) and benchmark catalyst IrO$_2$/C (60 mV/decade). This observation indicates the faster reaction kinetics of OER on MSQDs-AC as compared to the MSQDs before cycling and the state-of-art catalyst IrO$_2$/C. The activity of MSQDs-AC is compared with some of the state-of-the-art catalysts and other quantum dots for OER application and is summarized in Table S2. The Tafel slope of MSQDs-AC is comparable to other catalysts. The stability of the MSQDs electrocatalyst under the condition of oxygen evolution was tested through chronopotentiometry measurement at a constant current density of 10 mA/cm^2 (Figure 4D). After continuous electrolysis for 2 hr, very nominal change in the overpotential was observed reflecting its robustness for long-term reaction and will find promising application in the real field. A movie recorded during the oxygen evolution from the MSQDs-AC on glassy carbon plate electrode during electrolysis at overpotential 370 mV (@ 10 mA/cm^2) is presented in Movie S1 in the supporting information.

To gain further insight on the OER catalytic mechanism, we carried out the first-principles calculations. As in our previous work,[47] the computational modeling of the reactants, intermediates and products and reaction process involved in OER process was performed by using density functional theory (DFT) within the RPBE[48] exchange-correlation functional, as implemented in the Atomistix ToolKit.[49] The details of the computational method are presented in the supporting information.
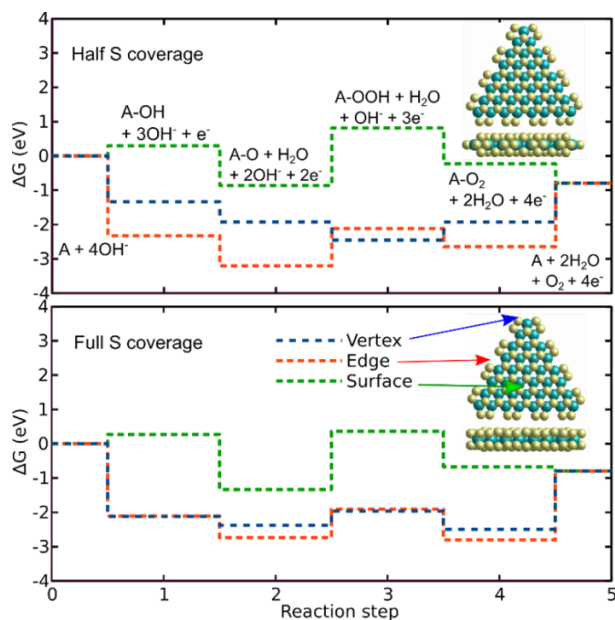

Figure 5. Free energy profiles for OER on vertex, edge and surface of MSQDs with Mo-edge and half/full S coverage, as revealed by first-principles calculations. The results are obtained at external potential U = 0.6 V and pH = 14.

The OER reaction mechanisms of the MSQDs were analyzed for different bias potentials by showing the profiles of free energy changes of the intermediates and products. For an electrocatalytic reaction, the catalytic performance may depend on the particular surface or edge termination at a given applied bias value. Therefore, the MSQDs with various edge terminations were considered (Figure S4), which have been observed in the experiments[50]. The results showed that the Mo edges are energetically more stable than the S edge for different size of MSQDs. This is in agreement with the earlier experimental results using scanning tunneling microscopy (STM) reported by Besenbacher et al.[51,52] and first-principles calculations.[53] Therefore, we have focused on QDs with Mo edges (full and half S coverage) for this study. For both types of the Mo edges, different possibilities of adsorption positions (at least 3) have been considered and the most stable structures have been used for free energy calculations (Figure S5). We have also studied the effect of vacancies on the surface and on the edges of MSQDs on the catalytic activity of these materials. The free energy changes of the intermediates and products under the catalytic roles of MSQDs are shown in Figure S6. It can be seen that the complete process is not favorable from the thermodynamic point of view without a potential bias to drive the reaction. The limiting step of the reaction, i.e., the one with the highest energy barrier, corresponds to the combination of OH$^-$ group with an adsorbed O atom for the formation of OOH species, except for vertex position where the highest barrier originates from dissociation of O$_2$ molecule from the MSQD. In general, the ΔG value of the rate-determining step indicates the rate of whole OER, and smaller ΔG suggests the lower energy barriers of intermediates and consequently faster OER process. The overall potentials obtained for OER process using MSQDs with different edge terminations and adsorption sites are summarized in Table S3. The results show lower activation barrier for the Mo edges containing half sulfur coverage than full sulfur coverage. Moreover, adsorption at vertex position shows the lowest overpotential in comparison to edges or surface. The highest overpotential is found for surface adsorption suggesting that MSQD plane is almost inactive during OER process, as suggested before from the experiment[51] and theory[54]. According to our results in the free-energy diagram (Figure 5), an external potential of U = 0.6 V is required to make the OER an exothermic reaction. The results show that the thermodynamic activation energy for the final step is higher for the edge or the vertex adsorption than the surface adsorption. The reason is the strong binding energy of oxygen molecule at edge and vertex positions, which require higher desorption energy in comparison to surface adsorption. According to the reaction process, the final step does not entail electron-transfer processes and, thus, the free energy step does not depend on the electrode potential. However, the binding energy of the molecule on MSQD decreases by growing the repulsion interaction between adsorbed oxygen molecules, which helps the oxygen molecule to escape from the surface and facilitates the recovery of the catalysts for the next cycle. Figure S7 shows the effect of the single sulfur vacancy on the OER processes. The vacancy positions were varied with respect to the perfect MSQD to reveal the effect of adsorption sites. As expected, the defects can significantly change the free energy diagram for all adsorption sites. In the case of Mo-edge with full S coverage, the overpotential decreases in both vertex and edge

positions (see Table S3) due to the enhanced adsorption strength on the vacancy site. Thus, our DFT calculations validate the assumption that the as-synthesized small MoS_2 quantum structures have defects at the edges and confirms the enhanced activity towards OER.

This enhanced electrocatalytic performance of the as-synthesized MSQDs was further accessed by estimating the double layer capacitance (C_{dl}) and roughness factor (R_f) of the materials. The C_{dl} and the R_f are directly proportional to the active surface area of the electrocatalyst and reflect the electrocatalytic performance of the materials.[13,18,20] The CV of the catalysts at different scan rates and the plot of current (i) vs scan rate (v) have been obtained (Figure S8). The C_{dl} and R_f values of the materials have been summarized in Table S4. As expected, the calculated C_{dl} value of IrO_2/C is higher than that in MSQDs. Interestingly, the MSQDs after activation show higher C_{dl} and R_f values as compared to the materials before the cycle and pristine MoS_2. So it clear evidence that the potential cycling of the MSQDs produces more active sites and increases the accessibility of –OH ions for oxidation to evolve the oxygen molecules. It reveals the new electrocatalytic process which may further develop for utilization of electrochemically active sites to enhance the performance of OER without any additives into the matrix of MSQDs.

To gain insight into the intrinsic catalytic activity of MSQDs after potential cycling, the number n of active sites and turn over frequency (TOF) were estimated.[55-57] The details of the calculation are discussed in the supporting information.
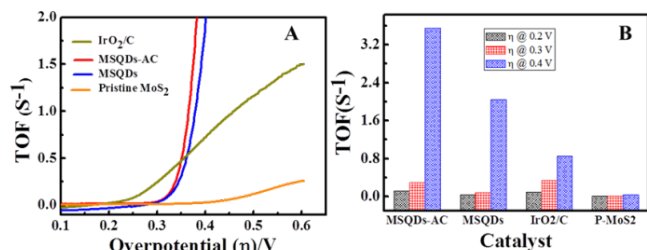

Figure 3. (A) TOF plot of different as-synthesized catalysts towards OER and (B) corresponding TOF values at different overpotential.

The values of n were calculated from the cyclic voltammetry (CV) data in the potential range from -0.2 V to +0.6 V vs RHE in 1M phosphate buffer (pH=7) at 50 mV/s (Figure S9). n is directly proportional to the integrated charge (Q_{cv}) obtained from the CV measurement, and it was derived using the equation 2 (supporting information). The value of n was estimated for all the electrocatalysts (Table S5). Then, the TOF value was derived using the equation 3 (supporting information). Assuming that all the materials on the modified electrode surface are catalytically active towards OER, the turnover frequency (TOF) was estimated and presented against the overpotential (Figure 6A). The TOF values of the catalysts have been compared at different overpotential (Figure 6B). The present observation validates that the activation of MSQDs by potential cycling dramatically influence the OER performance. The activation of MSQDs increased the TOF value.

MSQDs adds unavoidable CQDs to the solution.[32] The use of carbon-containing solvents contributes to the formation of CQDs during the synthesis process. However, the effects of unwanted CQDs on the application of MSQDs have not yet

been assessed. Therefore, a control experiment was designed using the mixture of organic solvent (DMF) and water to check any formation of carbon quantum dots (CQDs) at similar synthesis condition. The as-prepared sample was characterized by the UV-visible spectroscopy and irradiation of UV light. Surprisingly, the as-prepared solution showed the absorption band at ~330 nm and displayed greenish fluorescence under the irradiation of a 365 nm UV lamp (Figure S10). This observation confirms the formation of CQDs from the solvent containing carbon source. Then, the MSQDs have been synthesized in similar condition adding the DMF to the reaction medium deliberately to generate CQDs. So, it can be deduced that the as-synthesized solution contains the mixture of MSQDs and CQDs (MSQDs@CQDs). The synthesis schemes of the sample are presented in Figure S11. It showed the absorption band at ~295 nm and displayed bluish-green fluorescence under the irradiation of a 365 nm UV lamp (Figure S10). Interestingly, as synthesized samples of CQDs, MSQDs@CQDs and MSQDs show a variation in the UV-visible spectral pattern and fluorescence color during the irradiation of UV lamp (Figure S10). Furthermore, the influence of carbon quantum dots (CQDs) on the OER performance of MSQDs has been explored. It has been observed that the presence of some organic solvents generates CQDs, and also influence the UV and fluorescence properties. It is essential to understand the effect of unavoidable CQDs on the catalytic activity of MSQDs so that the synthesis strategy can be tuned. Therefore, the OER performance of as-synthesized CQDs, the mixture of MSQDs and CQDs (MSQDs@CQDs) has been explored and compared with the MSQDs. A substantial difference in the OER performance was observed (Figure S12). It indicates that CQDs suppress the OER performance of MSQDs. It can be speculated here that the CQDs have poor OER activity in comparison to MSQDs and their presence may block the active sites of MSQDs and hamper the catalytic performance. The measurement of the Tafel slopes validates the observation (Figure S12B). The Tafel slopes of MSQDs are lower as compared to the CQDs and MSQDs@CQDs. The present observation evidently provides a new insight to design the MSQDs free of CQDs for essential OER applications of interest. The C_{dl} and R_f values of the CQDs and MSQDs@CQDs have been derived to deduce the information on any correlation of the change in active surface areas (Figure S13). Interestingly, the C_{dl} and R_f values of the CQDs and MSQDs@CQDs are much lower than the MSQDs (Table S6). From here, it can be deduced that the presence of CQDs probably decreases the number of active sites in MSQDs or CQDs may be a barrier in approaching the reactant species on the surface. In order to understand the effects of carbon adsorption on the catalytic activity of the MSQDs, we have also studied the coverage of the QDs with a graphene flake (Figure S14). The optimized average interlayer distance (d) is 3.18 Å, which is in very good agreement with the previous value reported for the MoS_2/graphene heterostructures.[58] The Mulliken population analyses were used to evaluate the change of atomic charges (Δq) on the graphene flake before and after adsorption on the QD. It was found that the atomic charge is changed only by ~ 0.1 % per carbon atom indicating negligible charge transfer between the graphene flake and the MSQDs. Therefore, it is expected that introducing carbon into the MSQDs will not change the catalytic activity on the edge and the vertex adsorption but it can affect the adsorption of reaction intermediates on the QD's surface.

In summary, MSQDs have been successfully synthesized by a facial one-step hydrothermal method adopting a strategy to ignore the formation of unavoidable CQDs. The as-synthesized MSQDs have a very small lateral size ranging from 2 nm to 5 nm. Due to the strong quantum confinement, MSQDs exhibit a noticeable blue shift in the UV-visible absorption and PL-spectra. Remarkably, the MSQDs show excellent electrocatalyst activity towards OER, and our experimental and theoretical data provide insights into the OER activity. The theoretical results showed that the MoS_2 basal plane is almost inert during the OER process, while the OER reactivity occurs preferentially at the vertexes. If the number of vertexes remains constant for different sizes of MSQDs, the results suggest that the OER efficiency can be improved by reducing the lateral size of the QDs. Sulfur vacancies and their positions play an important role in the catalytic activity of MoS_2 QDs. As an example, single vacancies can create active sites at the edge and vertex of the QD with full S coverage, which can improve the OER performance. Also, a detailed experimental and theoretical insight on the presence of CQDs with the active sites of the MSQDs for OER has been obtained. It was revealed that the CQDs affect the adsorption of reaction intermediates on the MSQDs and suppress the electrocatalytic process of OER. Our findings provide important insights into the synthesis process of MSQDs and their catalytic properties so that these structures can be tuned for the use in promising energy applications.

AUTHOR INFORMATION

Corresponding Author

* bikash@immt.res.in; arkady.krasheninnikov@aalto.fi; mahdi.ghorbani@hzdr.de

Notes
The authors declare no competing financial interests.

ASSOCIATED CONTENT

Supporting Information. Experimental and computational details, XPS data, LSV Polarization plot at different potential cycles, Tables showing the summarized data, synthesis scheme and other related CV measurements. This material is available free of charge via the Internet at http://pubs.acs.org.

ACKNOWLEDGMENT

REFERENCES

(1) Dresselhaus, M. S.; Thomas, I. L. *Nature* **2001**, *414*, 332–337.

(2) Turner, J. A. *Science* **1999**, *285*, 687–689.

(3) Chow, J.; Kopp, R. J.; Portney, P. R. *Science* **2003**, *302*, 1528–1531.

(4) Li, Y.; Gong, M.; Liang, Y.; Feng, J.; Kim, J.-E.; Wang, H.; Hong, G.; Zhang, B.; Dai, H. *Nat. Commun.* **2013**, *4*, 1805-1812.

(5) Katsounaros, I.; Cherevko, S.; Zeradjanin, A. R.; Mayrhofer, K. J. *J. Angew. Chem. Int. Ed.* **2014**, *53*, 102–121.

(6) McCrory, C. C. L.; Jung, S.; Peters, J. C.; Jaramillo, T. F. *J. Am. Chem. Soc.* **2013**, *135*, 16977–16987.

(7) Gao, M.; Sheng, W.; Zhuang, Z.; Fang, Q.; Gu, S.; Jiang, J.; Yan, Y. *J. Am. Chem. Soc.* **2014**, *136*, 7077–7084.

(8) Gerken, J. B.; McAlpin, J. G.; Chen, J. Y. C.; Rigsby, M. L.; Casey, W. H.; Britt, R. D.; Stahl, S. S. *J. Am. Chem. Soc.* **2011**, *133*, 14431–14442.

(9) Lu, Z.; Chen, G.; Li, Y.; Wang, H.; Xie, J.; Liao, L.; Liu, C.; Liu, Y.; Wu, T.; Li, Y.; Luntz, A. C.; Bajdich, M.; Cui, Y. *J. Am. Chem. Soc.* **2017**, *139*, 6270–6276.

(10) Grimaud, A.; Diaz-Morales, O.; Han, B.; Hong, W. T.; Lee, Y.-L.; Giordano, L.; Stoerzinger, K. A.; Koper, M. T. M.; Shao-Horn, Y. *Nat. Chem.* **2017**, *9*, 457–465.

(11) Duan, H.; Li, D.; Tang, Y.; He, Y.; Ji, S.; Wang, R.; Lv, H.; Lopes, P. P.; Paulikas, A. P.; Li, H.; Mao, S. X.; Wang, C.; Markovic, N. M.; Li, J.; Stamenkovic, V. R.; Li, Y. *J. Am. Chem. Soc.* **2017**, *139*, 5494–5502.

(12) Popczun, E. J.; McKone, J. R.; Read, C. G.; Biacchi, A. J.; Wiltrout, A. M.; Lewis, N. S.; Schaak, R. E. *J. Am. Chem. Soc* **2013**, *135*, 9267–9270.

(13) Dutta, A.; Samantara, A. K.; Dutta, S. K.; Jena, B. K.; Pradhan, N. *ACS Energy Lett.* **2016**, *1*, 169–174.

(14) Dutta, A.; Pradhan, N. *J. Phys. Chem. Lett.* **2017**, *8*, 144–152.

(15) Zhou, W.; Wu, X.-J.; Cao, X.; Huang, X.; Tan, C.; Tian, J.; Liu, H.; Wang, J.; Zhang, H. *Energy Environ. Sci.* **2013**, *6*, 2921–2924.

(16) Voiry, D.; Fullon, R.; Yang, J.; de Carvalho Castro e Silva, C.; Kappera, R.; Bozkurt, I.; Kaplan, D.; Lagos, M. J.; Batson, P. E.; Gupta, G.; Mohite, A. D.; Dong, L.; Er, D.; Shenoy, V. B.; Asefa, T.; Chhowalla, M. *Nat. Mater.* **2016**, *15*, 1003–1009.

(17) Ganesan, P.; Prabu, M.; Sanetuntikul, J.; Shanmugam, S. *ACS Catal.* **2015**, *5*, 3625–3637.

(18) Xia, C.; Jiang, Q.; Zhao, C.; Hedhili, M. N.; Alshareef, H. N. *Adv. Mater.* **2016**, *28*, 77–85.

(19) Kong, D.; Wang, H.; Lu, Z.; Cui, Y. *J. Am. Chem. Soc.* **2014**, *136*, 4897–4900.

(20) Swesi, A. T.; Masud, J.; Nath, M. *Energy Environ. Sci.* **2016**, *9*, 1771–1782.

(21) Chen, H.; Wen, X.; Zhang, J.; Wu, T.; Gong, Y.; Zhang, X.; Yuan, J.; Yi, C.; Lou, J.; Ajayan, P. M.; Zhuang, W.; Zhang, G.; Zheng, J. *Nat. Commun.* **2016**, *7*, 12512.

(22) Behura, S.; Nguyen, P.; Che, S.; Debbarma, R.; Berry, V. *J. Am. Chem. Soc.* **2015**, *137*, 13060–13065.

(23) Chhowalla, M.; Shin, H. S.; Eda, G.; Li, L.-J.; Loh, K. P.; Zhang, H. *Nat. Chem.* **2013**, *5*, 263–275.

(24) Feldman, Y.; Frey, G. L.; Homyonfer, M.; Lyakhovitskaya, V.; Margulis, L.; Cohen, H.; Hodes, G.; Hutchison, J. L.; Tenne, R. *J. Am. Chem. Soc.* **1996**, *118*, 5362–5367.

(25) Laursen, A. B.; Kegnaes, S.; Dahl, S.; Chorkendorff, I. *Energy Environ. Sci.* **2012**, *5*, 5577–5591.

(26) Kamila, S.; Mohanty, B.; Samantara, A. K.; Guha, P.; Ghosh, A.; Jena, B.; Satyam, P. V; Mishra, B. K.; Jena, B. K. *Sci. Rep.* **2017**, *7*, 8378.

(27) Wu, J.; Liu, M.; Chatterjee, K.; Hackenberg, K. P.; Shen, J.; Zou, X.; Yan, Y.; Gu, J.; Yang, Y.; Lou, J.; Ajayan, P. M. *Adv. Mater. Interfaces.* **2016**, *3*, 1500669–1500675.

(28) Yan, K.; Lu, Y. *Small* **2016**, *12*, 2975–2981.

(29) Jaramillo, T. F.; Jørgensen, K. P.; Bonde, J.; Nielsen, J. H.; Horch, S.; Chorkendorff, I. *Science* **2007**, *317*, 100–102.

(30) Gopalakrishnan, D.; Damien, D.; Li, B.; Gullappalli, H.; Pillai, V. K.; Ajayan, P. M.; Shaijumon, M. M. *Chem. Commun.* **2015**, *51*, 6293–6296.

(31) Xu, S.; Li, D.; Wu, P. *Adv. Funct. Mater.* **2015**, *25*, 1127–1136.

(32) Jiang, L.; Zeng, H. *Nanoscale,* **2015**, *7*, 4580–4583.

(33) Xi, Y.; Serna, M. I.; Cheng, L.; Gao, Y.; Baniasadi, M.; Rodriguez-Davila, R.; Kim, J.; Quevedo-Lopez, M. A.; Minary-Jolandan, M. *J. Mater. Chem. C* **2015**, *3*, 3842–3847.

(34) Yuwen, L.; Yu, H.; Yang, X.; Zhou, J.; Zhang, Q.; Zhang, Y.; Luo, Z.; Su, S.; Wang, L. *Chem. Commun.* **2016**, *52*, 529–532.

(35) Gao, D.; Si, M.; Li, J.; Zhang, J.; Zhang, Z.; Yang, Z.; Xue, D.

Nanoscale Res. Lett. **2013**, *8*, 1–8.

(36) Yufit, V.; Nathan, M.; Golodnitsky, D.; Peled, E. *J. Power Sources.* **2003**, *122*, 169–173.

(37) Ambrosi, A.; Sofer, Z.; Pumera, M. *Small.* **2015**, *11*, 605–612.

(38) Sundaram, R. S.; Engel, M.; Lombardo, A.; Krupke, R.; Ferrari, A. C.; Avouris, P.; Steiner, M. *Nano Lett.* **2013**, *13*, 1416–1421.

(39) Lee, C.; Yan, H.; Brus, L. E.; Heinz, T. F.; Hone, J.; Ryu, S. *ACS Nano* **2010**, *4*, 2695–2700.

(40) Gao, M.-R.; Chan, M. K. Y.; Sun, Y. *Nat. Commun.* **2015**, *6*, 7493.

(41) Wilcoxon, J. P.; Samara, G. A. *Phys. Rev. B* **1995**, *51*, 7299–7302.

(42) Kioseoglou, G.; Hanbicki, A. T.; Currie, M.; Friedman, A. L.; Gunlycke, D.; Jonker, B. T. *Appl. Phys. Lett.* **2012**, *101,* 101906-101909.

(43) Ha, H. D.; Han, D. J.; Choi, J. S.; Park, M.; Seo, T. S. *Small* **2014**, *10*, 3858–3862.

(44) Stengl, V.; Henych, J. *Nanoscale* **2013**, *5*, 3387–3394.

(45) Khairutdinov, R. F.; Rubtsova, N. A.; Costa, S. M. B. *J. Lumin.* **1996**, *68*, 299–311.

(46) Browne, M. P.; Nolan, H.; Duesberg, G. S.; Colavita, P. E.; Lyons, M. E. G. ACS Catal. **2016**, *6*, 2408–2415.

(47) Kaukonen, M.; Krasheninnikov, A. V; Kauppinen, E.; Nieminen, R. M. *ACS Catal.* **2013**, *3*, 159–165.

(48) Perdew, J. P.; Burke, K.; Ernzerhof, M. *Phys. Rev. Lett.* **1998**, *80*, 891-891.

(49) McCarthy, C. L.; Downes, C. A.; Brutchey, R. L. *Inorg. Chem.* **2017**, *56*, 10143–10146.

(50) Kooyman, P. J.; van Veen, J. A. R. *Catal. Today* **2008**, *130*, 135–138.

(51) Lauritsen, J. V; Kibsgaard, J.; Helveg, S.; Topsoe, H.; Clausen, B. S.; Laegsgaard, E.; Besenbacher, F. *Nat. Nanotechnol.* **2007**, *2*, 53–58.

(52) Bollinger, M. V; Lauritsen, J. V; Jacobsen, K. W.; Nørskov, J. K.; Helveg, S.; Besenbacher, F. *Phys. Rev. Lett.* **2001**, *87*, 196803-196807.

(53) Cuddy, M. J.; Arkill, K. P.; Wang, Z. W.; Komsa, H.-P.; Krasheninnikov, A. V; Palmer, R. E. *Nanoscale* **2014**, *6*, 12463–12469.

(54) Raybaud, P.; Hafner, J.; Kresse, G.; Kasztelan, S.; Toulhoat, H. *J. Catal.* **2000**, *189*, 129–146.

(55) An, L.; Huang, L.; Zhou, P.; Yin, J.; Liu, H.; Xi, P. *Adv. Funct. Mater.* **2015**, *25*, 6814–6822.

(56) Gao, M.-R.; Cao, X.; Gao, Q.; Xu, Y.-F.; Zheng, Y.-R.; Jiang, J.; Yu, S.-H. *ACS Nano* **2014**, *8*, 3970–3978.

(57) Merki, D.; Fierro, S.; Vrubel, H.; Hu, X. *Chem. Sci.* **2011**, *2*, 1262–1267.

(58) Ghorbani-Asl, M.; Bristowe, P. D.; Koziol, K.; Heine, T.; Kuc, A. *2D Mater.* **2016**, *3*, 25018-25034.

Insert Table of Contents artwork here